Barton, D. A. W., Krauskopf, B., & Wilson, R. E. (2006). Homoclinic snaking in a neutral delay model of a transmission line oscillator.

Homoclinic snaking in a neutral delay model of a transmission line oscillator

David A W Barton, Bernd Krauskopf and R Eddie Wilson

Bristol Centre for Applied Nonlinear Mathematics, Department of Engineering Mathematics, University of Bristol, Queen's Building, Bristol, BS8 1TR, UK

E-mail: david.barton.99@bristol.ac.uk

Abstract. In a transmission line oscillator (TLO) a linear wave travels along a piece of cable, the transmission line, and interacts with terminating electrical components. A fixed time delay arises due to the transmission time through the transmission line. Recent experiments on a TLO driven by a negative resistor demonstrated rich delay-induced dynamics and high-frequency chaotic behaviour. Furthermore, good agreement was found with a neutral delay differential equation (NDDE) model.

In this paper we perform a numerical bifurcation analysis of the NDDE model of the TLO. Our main focus is on homoclinic orbits, which give rise to complicated dynamics and bifurcations. For small time delay there is a homoclinic orbit to a steady-state. However, past a codimension-two Shil'nikov-Hopf bifurcation the homoclinic orbit connects to a saddle-type periodic solution, which exists in a region bounded by homoclinic tangencies. Both types of homoclinic bifurcations are associated with snaking branches of periodic solutions. We summarise our results in a two-parameter bifurcation diagram in the plane of resistance against time delay.

Our study demonstrates that the theory of homoclinic bifurcations in ordinary differential equations largely carries over to NDDEs. However, we find that the neutral delay nature of the problem influences some bifurcations, especially convergence rates of homoclinic snaking.

AMS classification scheme numbers: 34K13, 34K18, 34K40, 34K60, 37C29

1. Introduction

Transmission line oscillators (TLOs) are simple electrical circuits that provide a rich source of delay-induced dynamics. TLOs consist of a transmission line, e.g. a coaxial cable, terminated by one or more nonlinear electrical components, e.g. Chua's diode [1, 2] or a tunnel diode [3]. Voltage waves propagate along the transmission line and are reflected and distorted by the terminating components. The simplicity of these circuits has made them of practical interest for many decades [4, 3, 5], and yet many open questions remain regarding the dynamics that they exhibit.

In this paper we present a systematic study of a TLO as modelled by a *neutral delay differential equation* (NDDE). In experiments, this TLO was found to produce chaotic high-frequency output [6, 7], which is of practical importance for applications such as communication [8, 9] and random signal radar/ladar [10]. We find that the dynamics of this TLO are organised by homoclinic bifurcations. As the delay time is increased, which corresponds to lengthening the transmission line, we see a transition from a homoclinic orbit of a steady-state to a homoclinic orbit of a periodic solution via a Shil'nikov-Hopf bifurcation.

This is accompanied by a significant increase in the complexity of the dynamics. In particular, we find the phenomenon of homoclinic snaking, where a stable periodic solution becomes homoclinic to another periodic solution of saddle-type. To our knowledge this is the first time that such dynamics have been found and studied in an NDDE. A better understanding of these dynamics may in future inform TLO design.

The model we study is given by

$$C\dot{u}(t) = -\left(\frac{1}{R_c} - \frac{1}{R}\right)u(t) + \left(\frac{1}{R_c} + \frac{1}{R}\right)g(u(t-\tau)) - Cg'(u(t-\tau))\dot{u}(t-\tau) \tag{1}$$

where $g(y)$ is defined implicitly by the unique solution of

$$-\frac{1}{R_c}[g(y) - y] = I_s(\exp((g(y)+y)/V_0) - 1). \tag{2}$$

Equation (1) describes the evolution of the voltage (measured with respect to ground) at one end of the transmission line, which is terminated by a negative resistor (with resistance R) in parallel with a capacitor (with capacitance C). The opposite end of the transmission line is terminated by a tunnel diode which is modelled by (2). A circuit diagram is shown in figure 1. The right-hand-side of (1) depends on the delayed dependent variable $u(t-\tau)$, and consequently (1) is a *delay differential equation* (DDE). The presence of the $\dot{u}(t-\tau)$ term means that (1) is in fact a *neutral delay differential equation* (NDDE). The delay time τ is the time taken for a voltage wave to travel along the entire length of the transmission line.

DDEs, that do not depend on the derivative of a delayed dependent variable, and NDDEs, that do, have many similar properties. To integrate forward in time an initial *function* is needed to specify the dependent variable on $t \in [-\tau, 0]$, where τ is the largest delay time. This is in contrast to ordinary differential equations (ODEs) which require a single initial value in $\mathbb{R}^n$ at $t = 0$. Despite this infinite-dimensional nature, bifurcations of DDEs are equivalent to bifurcations of suitable ODEs via centre manifold reduction [11]. This is because DDEs (with fixed delays) only have a point spectrum. However, this is not the case for NDDEs. The solutions of NDDEs possess an essential spectrum as well as a point spectrum and are able to undergo 'infinite dimensional' bifurcations. These are bifurcations that are not equivalent to any bifurcation in an ODE because the essential spectrum passes through the imaginary axis. In [12, 13] it is noted that such a bifurcation can create non-smooth periodic solutions.

Due to the technical difficulties associated with the analysis of NDDEs, only a limited number of mathematical tools have been used to investigate non-stationary behaviour in NDDE transmission line models. These tools include perturbation techniques [3], non-constructive proofs [14] and direct numerical simulation [15]. Other powerful tools that are widely used in the analysis of ODEs, such as numerical continuation (e.g. AUTO [16]), have not been exploited as these tools are under-developed for NDDEs. Numerical continuation enables the solutions of an equation to be followed in parameters to trace out solution branches. Further, bifurcations on branches can be detected and followed in two (or more) parameters. Thus, a global picture of the dynamics of a system can be built up systematically. Recently, numerical continuation software for DDEs has been developed in the form of DDE-BIFTOOL [17] and PDDE-CONT [18]. Subsequently, we have extended DDE-BIFTOOL to cover the case of NDDEs [19, 20]. We make use of this new tool to investigate the complicated behaviour exhibited by the TLO (1).

The paper proceeds as follows. We present the derivation of the model (1) along with an analysis of its steady-states in section 2. The trivial steady-state is unstable for all relevant parameter values. We find that there exists a single non-trivial steady-state, which is stable for high values of the resistance R. As R is decreased it loses stability at a supercritical Hopf bifurcation, and we show that in the (R, τ)-plane there exist infinitely many more curves

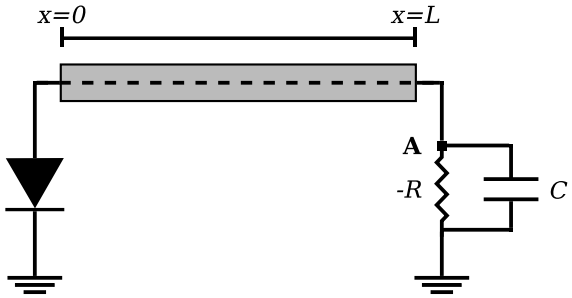

Figure 1. Circuit diagram of the TLO implemented by Blakely and Corron [6]. The transmission line is shown in grey. It is terminated on the left by a tunnel diode and on the right by a negative resistor in parallel with a capacitor.

of Hopf bifurcations. Section 3 contains some background material on homoclinic orbits and homoclinic snaking. We also describe in detail the numerical methods that we use to investigate the homoclinic orbits in one and two parameters. Then, in section 4 we show the existence of a homoclinic orbit the limit $\tau \to \infty$. Through numerical continuation of the associated snaking branches, we find that the homoclinic orbit is connected to the non-trivial steady-state of (1). In sections 5 and 6 we consider another homoclinic orbit that exists for finite τ, which for small τ is connected to the trivial steady-state of (1). It is in the vicinity of this homoclinic orbit that chaotic behaviour has been found experimentally. As τ is increased, the trivial steady-state undergoes a Shil'nikov-Hopf bifurcation and, consequently, the system develops a robust homoclinic orbit to a periodic solution. In section 6 we illustrate how the essential spectrum of the NDDE (1) causes slow convergence of the snaking branches of a homoclinic orbit connected to the trivial steady-state. Additionally, we show that the structure of snaking branches becomes more complicated as τ is increased; the periodic solution involved in the robust homoclinic orbit undergoes a period-doubling bifurcation. Furthermore, the possibility of further homoclinic orbits and heteroclinic connections arises. Our results are summarised in a two-parameter bifurcation diagram showing the domain of existence of the homoclinic orbits in the (R,τ)-plane. We then conclude with a discussion of some of the remaining open questions.

2. Derivation of the model

Figure 1 shows the circuit diagram of the transmission line oscillator (TLO) that we investigate. The TLO consists of a coaxial cable terminated by a diode at one end and by a negative resistor in parallel with a capacitor at the other end. Originally, it was modelled with a continuous time difference equation by Corti *et al* [21]. However, experimental results by Blakely and Corron [6] show that better correspondence between model and experiments is obtained when using the NDDE model (1).

We follow the model derivation of [6] and assume that the transmission line in figure 1 is lossless and governed by the Telegrapher's equations

$$\begin{aligned} R_c \frac{\partial I}{\partial t}(x,t) &= -v_0 \frac{\partial V}{\partial x}(x,t) \\ \frac{\partial V}{\partial t}(x,t) &= -v_0 R_c \frac{\partial I}{\partial x}(x,t) \end{aligned} \tag{3}$$

where I and V are the current and voltage along the transmission line, R_c is the characteristic

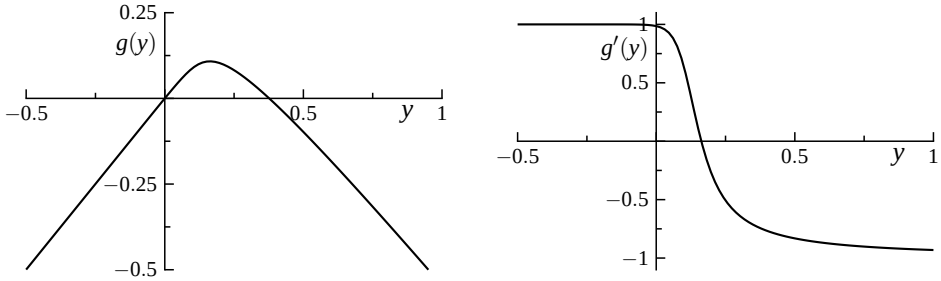

Figure 2. The function $g(y)$ and its first derivative $g'(y)$ as defined by (2).

impedance, and v_0 is the transmission speed along the transmission line. The diode, located at $x = 0$, provides the boundary condition

$$-I(0,t) = I_s(\exp(V(0,t)/V_0) - 1) \tag{4}$$

where I_s is the saturation current and V_0 is the threshold voltage. The second boundary condition, provided by the negative resistor and capacitor in parallel at $x = L$, is

$$C\frac{\partial V}{\partial t}(L,t) = I(L,t) + \frac{V(L,t)}{R} \tag{5}$$

where R is the resistance and C is the capacitance. The general solution of the hyperbolic system (3) is a D'Alembert solution of the form

$$\begin{aligned} V(z,t) &= \psi^{\mathrm{R}}(t - x/v_0) + \psi^{\mathrm{L}}(t + x/v_0) \\ I(z,t) &= (\psi^{\mathrm{R}}(t - x/v_0) - \psi^{\mathrm{L}}(t + x/v_0))/R_c \end{aligned} \tag{6}$$

where ψ^{L} and ψ^{R} are arbitrary functions. Substituting (6) into the boundary condition (4) gives the relation $\psi^{\mathrm{R}}(t) = g(\psi^{\mathrm{L}}(t))$; cf. (2). The function g and its first derivative g' are plotted in figure 2. We arrive at the final form, the NDDE (1), after substituting (6) and $\psi^{\mathrm{R}}(t) = g(\psi^{\mathrm{L}}(t))$ into the second boundary condition (5) and relabelling $\psi^{\mathrm{L}} =: u$ and $\tau := 2L/v_0$.

Throughout this paper we choose as the principle bifurcation parameters the resistance R and the time delay τ. These parameters are easily varied experimentally; the resistance is altered by the use of a variable resistor and the time delay is altered by the use of different lengths of coaxial cable. The parameter ranges under consideration are $40\,\Omega \le R \le 120\,\Omega$ and $0\,\mathrm{ns} \le \tau \le 20\,\mathrm{ns}$. For the remaining parameters we use the experimental values from [6], which are $C = 80\,\mathrm{pF}$, $R_c = 50\,\Omega$, $v_0 = 1.97 \times 10^8\,\mathrm{m/s}$, $I_s = 8\,\mu\mathrm{A}$, and $V_0 = 55\,\mathrm{mV}$.

Equation (1) has two steady-states in the parameter range of interest; the trivial solution $u(t) \equiv u_0 := 0$, and the non-trivial solution $u(t) \equiv u_1$ implicitly defined by $(R - R_c)/(R + R_c)u_1 = g(u_1)$. The stability of the steady-states is determined by the roots of the associated characteristic equation [22]

$$C\lambda + \left(\frac{1}{R_c} - \frac{1}{R}\right) + g'(u_{0,1})\exp(-\lambda\tau)\left(\lambda - \frac{1}{R_c} - \frac{1}{R}\right). \tag{7}$$

Hopf bifurcations of the steady-states occur at parameter values for which there exists a purely imaginary root of (7). To find these roots we make the substitution $\lambda = i\omega$ where $\omega \in \mathbb{R}$ and then separate real and imaginary parts to produce

$$\begin{aligned} 0 &= g'(u_{0,1})\left\{\left(\frac{1}{R_c} + \frac{1}{R}\right)\cos(\tau\omega) - C\omega\sin(\tau\omega)\right\} - \left(\frac{1}{R_c} - \frac{1}{R}\right) \\ 0 &= g'(u_{0,1})\left\{\left(\frac{1}{R_c} + \frac{1}{R}\right)\sin(\tau\omega) + C\omega\cos(\tau\omega)\right\} + C\omega. \end{aligned}$$

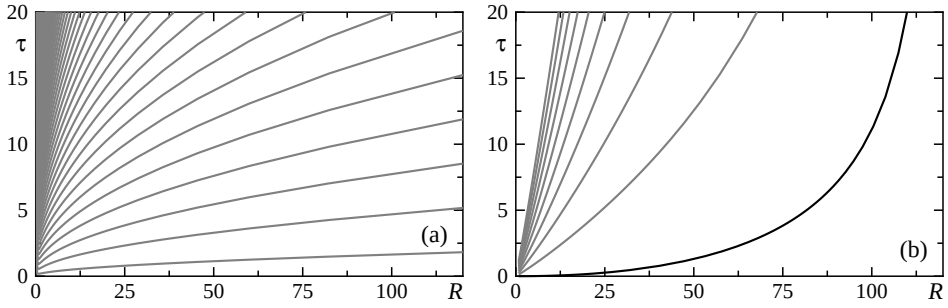

Figure 3. Curves of Hopf bifurcations of the trivial steady-state u_0 (a) and of the non-trivial steady-state u_1 (b). All Hopf bifurcations are supercritical; the rightmost Hopf curve in panel (b) from which a branch of stable periodic solutions emerges is marked in black.

For the trivial steady-state $u_0 = 0$ there exist infinitely many curves of Hopf bifurcations in the (R,τ)-plane. These curves, shown in figure 3(a), are parameterised by the Hopf frequency ω and given by

$$\tau(\omega) = \begin{cases} (2n\pi - \sin^{-1}(C\omega(1+(g(0))^2)/A) - B)/\omega \\ ((2n-1)\pi + \sin^{-1}(C\omega(1+(g(0))^2)/A) - B)/\omega \end{cases}$$

$$R(\omega,\tau) = -\frac{g'(0)\sin(\omega\tau)}{C\omega + g'(0)\sin(\omega\tau)/R_c + Cg'(0)\omega\cos(\omega\tau)}$$

where $n \in \mathbb{Z}$ and

$$A = 2(1/R_c^2 + C^2\omega^2)^{\frac{1}{2}}g'(0), \qquad B = \tan^{-1}(C\omega R_c).$$

All of the Hopf bifurcations on these curves are supercritical and the resulting branches of periodic solutions emerge in the direction of increasing τ. In the parameter region of interest, the trivial steady-state u_0 is always unstable.

Since u_1 is dependent on R and $g(u_1) \neq 0$, it is only possible to obtain implicit formulae for the Hopf bifurcation curves of the non-trivial steady-state u_1. The first ten curves of these Hopf bifurcations are shown in figure 3(b). All the Hopf curves shown in figure 3 (a) and (b) are found to be supercritical by numerical continuation. For large values of R the non-trivial steady-state u_1 is stable. Thus, when R is decreased, u_1 loses stability at the right-most Hopf curve shown in figure 3(b).

In the remainder of this paper we investigate the periodic solutions emerging at the Hopf bifurcations; in section 4 we focus on the periodic solutions bifurcating from u_0 and in sections 5 and 6 we focus on the periodic solutions bifurcating from u_1. The investigation of these periodic solutions gives key information regarding the homoclinic orbits of (1).

3. Background material on homoclinic orbits and numerical continuation

In many applications the dynamics are organised by homoclinic orbits; examples include the buckling of struts [23, 24], neuronal activity [25], water waves [26] and nonlinear optics [27]. The theory of homoclinic orbits is well developed for ODE models [28, 29, 30]. By contrast, homoclinic orbits in DDEs and NDDEs have not been widely studied. As is shown in this paper, the theory for ODEs to a large degree transfers to NDDEs. Here, we briefly recall some results regarding homoclinic orbits in generic systems of ODEs and we describe the associated numerical continuation techniques as used in later sections.

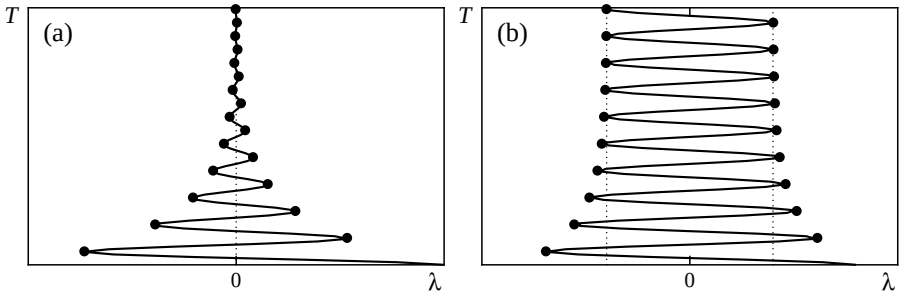

Figure 4. An illustration of two snaking branches of periodic solutions close to a homoclinic orbit of a saddle-focus type steady-state (a) and a homoclinic orbit of a periodic solution (b). Saddle-node bifurcations on the branches are marked by dots.

3.1. Homoclinic orbits

A homoclinic orbit of a system is given by the intersection of the stable and unstable manifolds of a saddle-type invariant set [28]. The stable manifold is defined as the set of all trajectories that tend to the invariant set in forward time, and the unstable manifold is defined as the set of all trajectories that tend to the invariant set in backward time. Here, the only invariant sets that we consider are steady-states and periodic solutions. A homoclinic orbit to a steady-state is of codimension one — it may be destroyed by small perturbations to the system parameters. (Throughout, we consider systems without special properties, such as symmetries.) However, a homoclinic orbit to a periodic solution is of codimension zero — the stable and unstable manifolds of the periodic solution intersect transversally and, consequently, the intersection persists under C^1 perturbations [28, Sec. 6.1 and 7.2.1]. A homoclinic orbit of a periodic solution can only be destroyed through a codimension-one *homoclinic tangency*. This occurs when the intersection of the stable and unstable manifolds becomes tangential and, thus, a small perturbation can separate the manifolds completely. A transition between a homoclinic orbit of a saddle-focus type steady-state and a homoclinic orbit of a periodic solution occurs at a codimension-two *Shil'nikov-Hopf bifurcation* [31]. At the Shil'nikov-Hopf bifurcation the homoclinic orbit is 'transfered' from the steady-state to the periodic solution. In two-parameter space this gives a transition from a one-dimensional locus (the codimension-one homoclinic orbit of a steady-state) to a two-dimensional area (the codimension-zero homoclinic orbit of a periodic solution); see figure 13.

In the vicinity of either kind of homoclinic orbit there may exist many additional periodic solutions [28, 32]. These periodic solutions can form *snaking branches* that undergo an infinite sequence of saddle-node bifurcations (or folds) as is sketched in figure 4. As a snaking branch is followed, the period of the periodic solution increases without limit as it becomes a better approximation to the homoclinic orbit itself. The two types of homoclinic orbits considered in this paper can be distinguished by the behaviour of the associated snaking branches as the period of the solutions tends to infinity. For a homoclinic orbit of a steady-state, the folds of the snaking branches converge exponentially quickly in parameter space to a single codimension-one point (see figure 4(a)), namely the homoclinic orbit itself. Conversely, for a homoclinic orbit of a periodic solution, the folds of the snaking branches converge (again exponentially quickly) to a pair of codimension-one points (see figure 4(b)), namely the homoclinic tangencies associated with the homoclinic orbit. Consequently, the snaking branches of a homoclinic orbit of a periodic solution remain of finite width in parameter space. In addition, a periodic solution of sufficiently large period at a fold of a snaking branch

can be used to approximate the respective homoclinic tangency.

Close to either type of homoclinic orbit (the *primary homoclinic orbit* or 1-homoclinic orbit) there may exist *secondary homoclinic orbits* or *n*-homoclinic orbits [28, 33]. These orbits make *n* global excursions before returning to the invariant set. Like the 1-homoclinic orbit, associated with each of these *n*-homoclinic orbits are snaking branches of periodic solutions. The snaking branches may not have the same structure as the snaking branches of the primary homoclinic orbit; instead they can form isolated branches or have a more complicated snaking structure. We refer to the solutions associated with the secondary homoclinic orbits as *multi-pulse solutions*.

3.2. Numerical continuation

Our principal tool for investigating (1) is numerical continuation, a technique by which solutions of an equation are followed in parameters to trace out continuous branches. Along these branches, bifurcations can be detected by monitoring the eigenvalues (or Floquet multipliers) of the solutions or by monitoring suitable test functions. General introductions to numerical continuation can be found in [34, 28, 35, 36].

Numerical continuation is firmly established for ODEs with many general purpose software packages in existence, e.g. [16, 37]. However, software packages to continue solutions of DDEs are comparatively new [17, 18] and extensions to deal with NDDEs even more so [19, 20]. For the continuation of periodic solutions in one parameter we use DDE-BIFTOOL [17] with extensions that we have developed for NDDEs [20]. DDE-BIFTOOL is a Matlab package that is capable of continuing steady-state and periodic solutions in one parameter as well as steady-state bifurcations in two parameters. Currently, it is unable to continue the bifurcations of periodic solutions. To continue saddle-node bifurcations we use LOCA (part of the Trilinos package) [38], again extended by us to deal with NDDEs. LOCA is a C++ library designed to continue the solutions of large systems of equations and their bifurcations.

It is common to plot one-parameter continuations against a projection of the solution. Throughout this paper we use the L_2-norm as defined by

$$\|u\| = \left(\int_0^1 u^2(t) \mathrm{d}t \right)^{\frac{1}{2}} \tag{8}$$

where the periodic solution u has been rescaled to the range $t \in [0,1]$.

For ODEs it is possible to continue homoclinic orbits of steady-state solutions directly as codimension-one bifurcations using AUTO/HomCont [16]. Although there is the added complication of an infinite-dimensional stable manifold, it is also possible to do this for DDEs with DDE-BIFTOOL [17, 39]. However, this capability has not yet been extended to include NDDEs. Also, we are not aware of any software that is capable of continuing homoclinic tangencies of periodic solutions in ODEs, DDEs or NDDEs. Consequently, we approximate the location in parameter space of the homoclinic orbits of steady-states and homoclinic tangencies of periodic solutions by continuing the folds of the associated snaking curve. As mentioned in the previous subsection, the convergence of the snaking region is exponential and so, by choosing a fold associated with a periodic solution whose period is large, we are able to approximate the homoclinic orbit/tangency accurately. To further ensure the accuracy of the continuation, we continue two consecutive folds in two parameters and monitor the discrepancy between them.

In sections 5 and 6 we consider homoclinic orbits where the underlying invariant set has one unstable eigenvalue/Floquet multiplier. Thus, we can approximate the unstable manifold

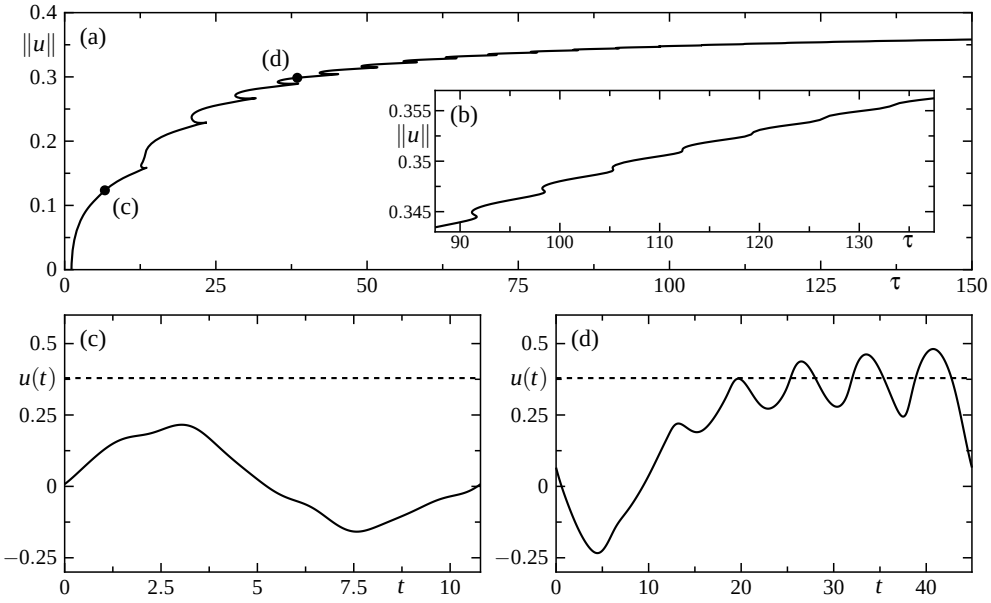

Figure 5. A one-parameter continuation in τ for fixed $R = 49.5$ of the unstable periodic orbit bifurcating from the trivial branch of steady-state solutions (a). As τ is increased, the series of fold bifurcations stops as is illustrated by the enlargement in panel (b). Panels (c) and (d) show time series at the points marked in panel (a). The nontrivial steady-state u_1 is marked on panels (c) and (d) by a dashed line.

using direct numerical integration. For this we use RADAR5, which is an implicit fourth order scheme with discontinuity tracking, specifically designed for stiff DDEs and NDDEs [40, 41, 42]. When the invariant set is a steady-state we integrate from initial points along its unstable eigenvector to approximate its one-dimensional unstable manifold. When the invariant set is a periodic solution (and so the unstable manifold is two-dimensional) we take a Poincaré section and integrate a sequence of points on an (approximate) fundamental domain of the corresponding return map. The fundamental domain is a small linear interval between a point on the unstable eigendirection and its image under the return map. Due to the spiralling nature of the domain, this provides a good representation of the two-dimensional unstable manifold.

4. Periodic solutions bifurcating from the trivial steady-state

In this section we consider the branches of periodic solutions emerging from the Hopf bifurcations of the trivial steady-state $u_0 = 0$. These branches are in fact all unstable but are of interest for building up a picture of the global dynamics of (1). In the limit $\tau \to \infty$, the solutions on these branches approach a homoclinic orbit of the non-trivial steady-state u_1. For finite (and small) τ, these solutions possess their own homoclinic orbit as will be discussed in section 5.

We begin our study of the bifurcating periodic solutions by performing one-parameter continuations with the time delay τ as the free parameter. Figure 5(a) shows the results of one such continuation for $R = 49.5$. The branch starts at the Hopf bifurcation at $\tau = 1.132$ and then, as τ is increased, undergoes two consecutive fold (or saddle-node) bifurcations.

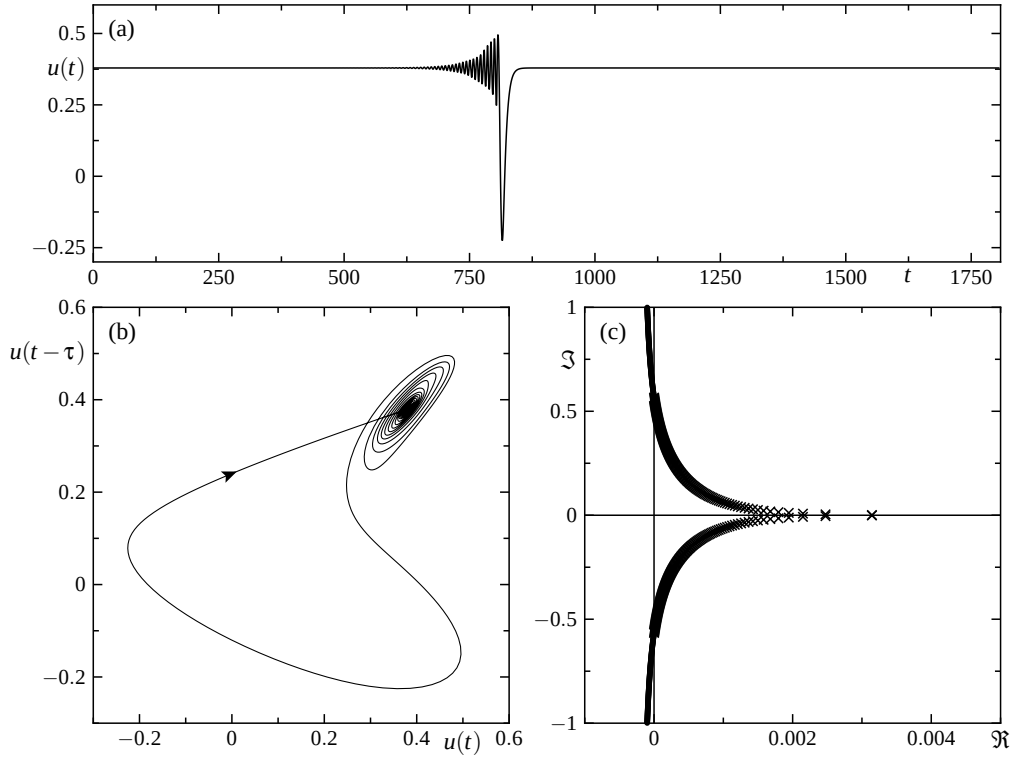

Figure 6. The time series of a periodic solution for $\tau = 1800$ and $R = 49.5$ is shown in panel (a), and its projection into the $(u(t), u(t-\tau))$-plane is shown in panel (b). Panel (c) shows the spectrum of the non-trivial steady-state u_1; stable eigenvalues ($\Re(\lambda) < 0$) are marked with a dot and unstable eigenvalues ($\Re(\lambda) > 0$) are marked with a cross.

When τ is increased, further pairs of folds occur in a very regular manner; each pair is almost equidistant in τ. These folds lead to a snake-like appearance that 'drifts' with the time delay. In fact the pairs of folds are not equidistant. Instead, as τ grows larger, the folds that make up a single pair grow closer until, for sufficiently large τ, they appear to have coalesced at a cusp bifurcation nearby in parameter space; see figure 5(b). For larger τ there are no further folds on the branch.

Panels (c) and (d) of figure 5 show the time series of two periodic solutions on the branch shown in panel 5(a). The periodic solution in figure 5(c) is close to the Hopf bifurcation and, consequently, it is centred around u_0. As the branch is followed, small oscillations appear in the solution profile as seen in figure 5(d). These oscillations appear to be centred around the non-trivial steady-state u_1, marked on the figure as a dashed line. As τ becomes larger, additional oscillations appear after every pair of folds on the branch. Each additional oscillation created is smaller than the previous one. When τ is sufficiently large so that there are no further folds on the branch, the process of adding oscillations still continues. The time series of a solution for $\tau = 1800$ with many small oscillations around u_1 is shown in figure 6(a). Although from the scale of the figure it appears that the solution is identical to u_1 for a finite length of time, in reality this is not the case; the solution always maintains an oscillatory component. Figure 6(b) shows the solution projected onto the $(u(t), u(t-\tau))$-plane, which illustrates how it slowly spirals out from u_1 before being re-injected close to

u_1.

The snake-like appearance of the branch of periodic solutions along with the behaviour of the solutions on it suggests that there exists a homoclinic orbit of u_1 in the limit $\tau \to \infty$. Indeed, the period of the solutions grows almost linearly with increasing τ. The eigenvalues of u_1 for $\tau = 1800$ are shown in figure 6(c). There are many complex conjugate pairs of unstable eigenvalues (crosses) and of stable eigenvalues (dots); these appear to align on a vertical asymptote in the complex plane. As τ increases, more pairs of complex conjugate eigenvalues pass into the right-hand-half of the complex plane.

5. Periodic solutions emerging from the non-trivial steady-state

In this section we investigate the stable periodic solutions that emerge from a Hopf bifurcation of the non-trivial steady-state u_1. In a similar fashion to the periodic solutions of the previous section we see snaking behaviour in the solution branch. However, in contrast we demonstrate the existence of a homoclinic orbit to a periodic solution. The snaking behaviour shown here occurs for finite and physically realisable values of τ. Additionally, many multi-pulse solutions are found and continued. Throughout this section we fix the time delay at $\tau = 3.5$; we extend the results to other values of τ in section 6.

Figure 7(a) shows a branch of periodic solutions with varying resistance R; snaking behaviour can clearly be seen. The branch is created at a super-critical Hopf bifurcation of u_1 when $R = 72.75$. Figure 7(b) shows an enlargement of panel (a) in the vicinity of the first fold. The solutions on the branch are locally stable until the period-doubling bifurcation PD_1. Continuation of the bifurcating branches of period-doubled solutions shows the existence of a sequence of period-doubling bifurcations, possibly leading to a period-doubling route to chaos. The branch regains stability at the period-doubling bifurcation PD_2 before losing stability again at the first fold bifurcation SL_1. This interplay between period-doubling bifurcations and saddle-node bifurcations is typical of homoclinic snaking in general [28].

In figure 8 we plot the same snaking branch in terms of the solution period T. The branch has an infinite sequence of folds (as the period increases monotonically) whose locations in R rapidly converge to one of two distinct values that correspond to homoclinic tangencies. The left-hand folds converge to $R = 48.69$ and the right-hand folds to $R = 50.52$. Between each of the consecutive left- and right-hand folds there exist two period-doubling bifurcations (not shown). All of the resulting period-doubled solutions that have been continued numerically appear to be qualitatively identical to those shown in figure 7. The branch in figure 8 was continued as far as is computationally tractable; the snake-like behaviour persisted over a near constant region of parameter space throughout. The behaviour shown in figure 8 is indicative of the existence of a robust homoclinic orbit of a periodic solution.

Figure 8 (a)–(f) are time series of several periodic solutions along the snaking branch. Near the base of the branch, i.e. where the period is small, the periodic solutions have a single local minimum/maximum. As the branch is followed (and the period of the solutions increases) the solutions gain additional local extrema in the vicinity of the left-hand folds. These local extrema are added in the form of additional small oscillations on the tail of the original large amplitude oscillation. When sufficiently many small oscillations have been added to the solution (e.g. figure 8(c)) the small oscillations are centred around u_0. Also, these small oscillations appear to follow the trajectory of an underlying periodic solution. Thus, as the snaking branch is followed, the periodic solution on the branch becomes an increasingly accurate approximation of a homoclinic orbit of the underlying saddle-type periodic solution.

The snaking behaviour of the branch in figure 8 is further illustrated in figure 9 with a sequence of periodic solutions along the branch in the $(u(t), u(t-\tau))$-plane. The periodic

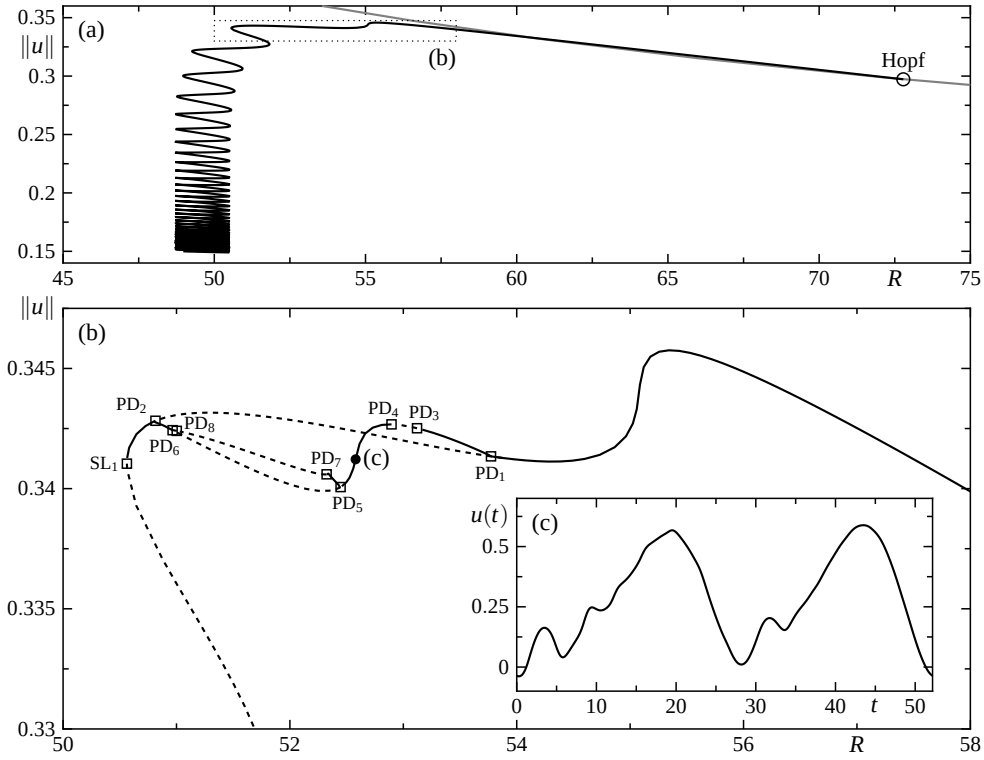

Figure 7. Branch of periodic solutions, for fixed $\tau = 3.5$, emerging from a Hopf bifurcation of u_1 is shown (a) and an enlargement in the vicinity of the first fold is shown (b). We fix $\tau = 3.5$. The solid curves in panel (b) indicate stable periodic solutions and the dashed curves indicate unstable periodic solutions. The branch undergoes a sequence of period-doubling bifurcations marked PD$_i$ before encountering the fold at SL$_1$. Some of the bifurcating branches of period-doubled solutions are shown; panel (c) contains a time series of the labelled period-doubled solution.

solutions on the snaking branch are labelled Γ_s and the underlying saddle-type periodic solution, to which the homoclinic orbit belongs, is labelled Γ_u. Away from the snaking region, the period of Γ_s is small [figure 9(a)]: Γ_u encircles the trivial steady-state u_0 and Γ_s encircles the non-trivial steady-state u_1. As the snaking region is approached and the period of Γ_s increases, Γ_s begins to deform and approach Γ_u [figure 9(b)]. Upon entering the snaking region, loops appear in the projection of Γ_s [figure 9(c)] in the vicinity of Γ_u. As the snaking branch is followed further, more loops are formed [figure 9(d–f)] that encompass Γ_u. As the period of the solutions tends to infinity, Γ_s makes many loops around Γ_u before making a global excursion around u_1 and returning to Γ_u. In other words, Γ_s approaches a homoclinic orbit to Γ_u. In figure 9 we find the periodic solution Γ_u by isolating a single loop of Γ_s of sufficiently high period. By performing a Newton iteration we find that Γ_u is part of a branch of periodic solutions that emerge from a Hopf bifurcation of u_0; it is the same branch of periodic solutions that was described in section 4.

As stated in section 3.1, the homoclinic orbit is defined by the intersection of the stable and unstable manifolds of Γ_u. DDE-BIFTOOL provides the Floquet multipliers of Γ_u: it has one unstable Floquet multiplier and thus a two-dimensional unstable manifold $W^u(\Gamma_u)$. We use the methods described in section 3.2 to approximate $W^u(\Gamma_u)$ and so further investigate

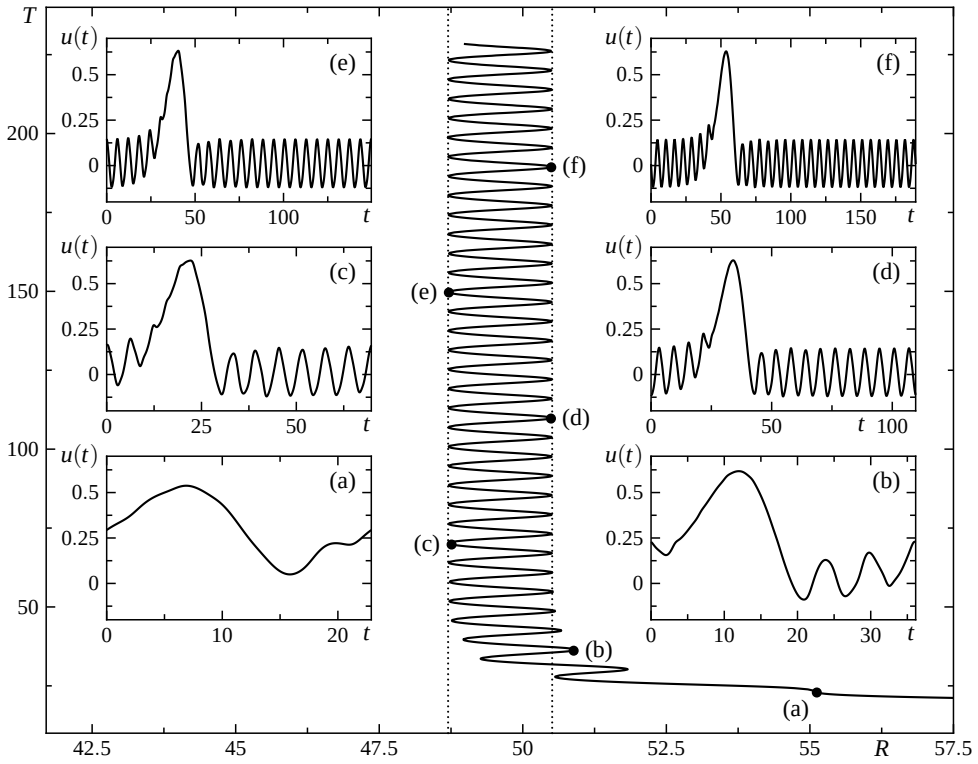

Figure 8. The main panel shows the continuation of the branch shown in figure 7, now projected into the (R,T)-plane, where T is the period of the solution. The folds of the branch rapidly converge to one of two parameter values (the homoclinic tangencies) as shown by the dotted lines in the figure. The panels (a)–(f) show time series of solutions along this branch at the labelled points.

the homoclinic orbit. Figure 10 shows $W^{\mathrm{u}}(\Gamma_{\mathrm{u}})$ projected onto the $(u(t),u(t-\tau))$-plane for $R = 49.5$ (the approximate centre of the snaking curve shown in figure 8). Figure 10(a) shows trajectories on $W^{\mathrm{u}}(\Gamma_{\mathrm{u}})$ that make one large excursion away from Γ_{u}, return to Γ_{u} and are then expelled in the opposite direction. In figure 10(b) we show trajectories that stay on the right-hand branch of $W^{\mathrm{u}}(\Gamma_{\mathrm{u}})$ for at least 180 ns; these trajectories make multiple large excursions away from Γ_{u} and then back to Γ_{u}. Note that the 'gaps' in one representation of $W^{\mathrm{u}}(\Gamma_{\mathrm{u}})$ correspond to the orbits in the other representation. In both figures we see that the solution trajectories stay close to the underlying periodic solution for a short time before spiralling away. The trajectories then curve around the non-trivial steady-state u_1 and are re-injected nearby Γ_{u}.

We expect there to exist infinitely many *multi-pulse orbits* where the orbit makes multiple global excursions away from Γ_{u}. Evidence for this is provided by trajectories that make multiple large excursions. We constructed multi-pulse solutions from segments of existing periodic solutions, which where then corrected with a Newton iteration. These are continued using DDE-BIFTOOL to trace out whole branches of multi-pulse solutions, as is shown in figure 11. The branches of multi-pulse solutions form disconnected islands of solutions which, as the period increases, become increasingly difficult to distinguish. (Indeed, they appear to be connected but this is an artifact of the projection.) Figure 12 shows the time series and

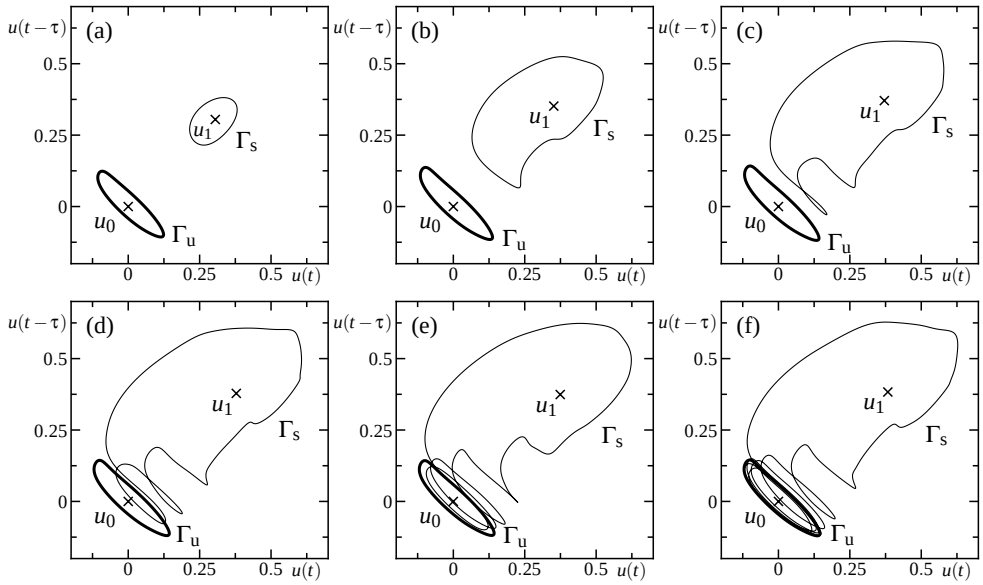

Figure 9. Projections onto the $(u(t), u(t-\tau))$-plane of snaking periodic solution Γ_s along the branch shown in figure 8(a). The periodic solution begins to 'wrap' around an underlying periodic solution Γ_u as the snaking branch is followed in the direction of increasing period T. The two crosses mark the two steady-state solutions u_0 and u_1.

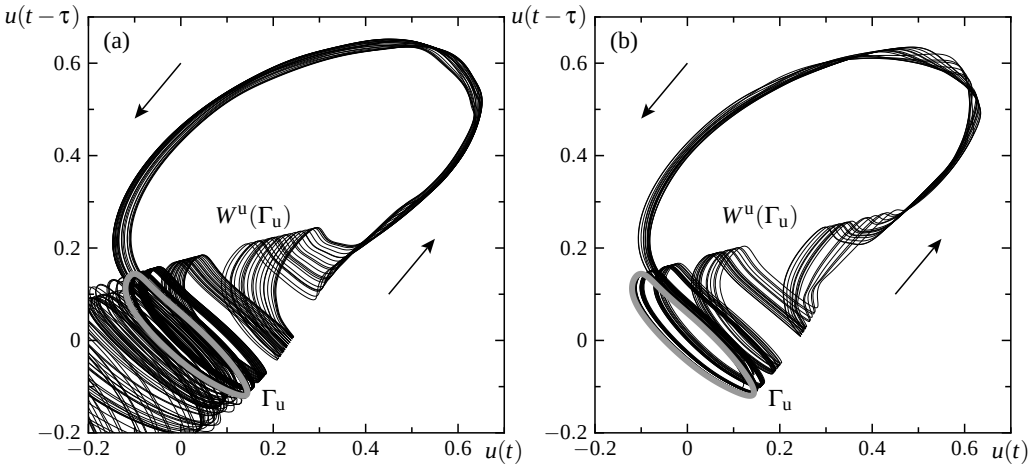

Figure 10. An approximation of $W^u(\Gamma_u)$ for $R = 49.5$. Panel (a) shows the trajectories along the unstable manifold that make one global excursion away from Γ_u before returning and being ejected in the opposite direction. Panel (b) shows the trajectories that make multiple global excursions away from and then back to Γ_u before being ejected in the opposite direction.

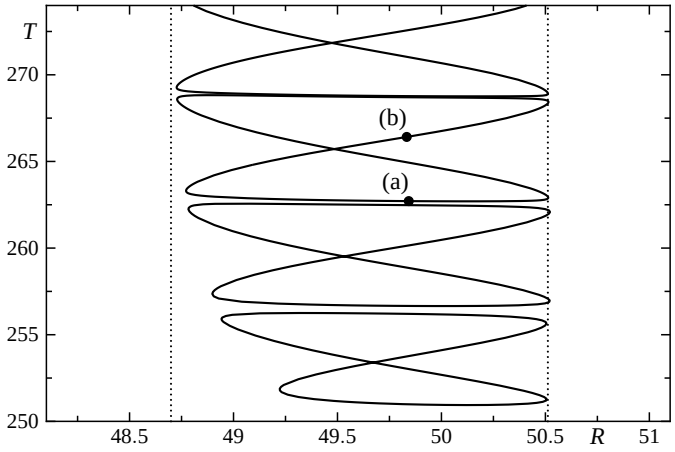

Figure 11. Branches of two-pulse periodic solutions, each forming disconnected islands. The points marked (a) and (b) correspond to the periodic solutions shown in figure 12. The dashed lines denote the locations of the homoclinic tangencies of the primary homoclinic orbit.

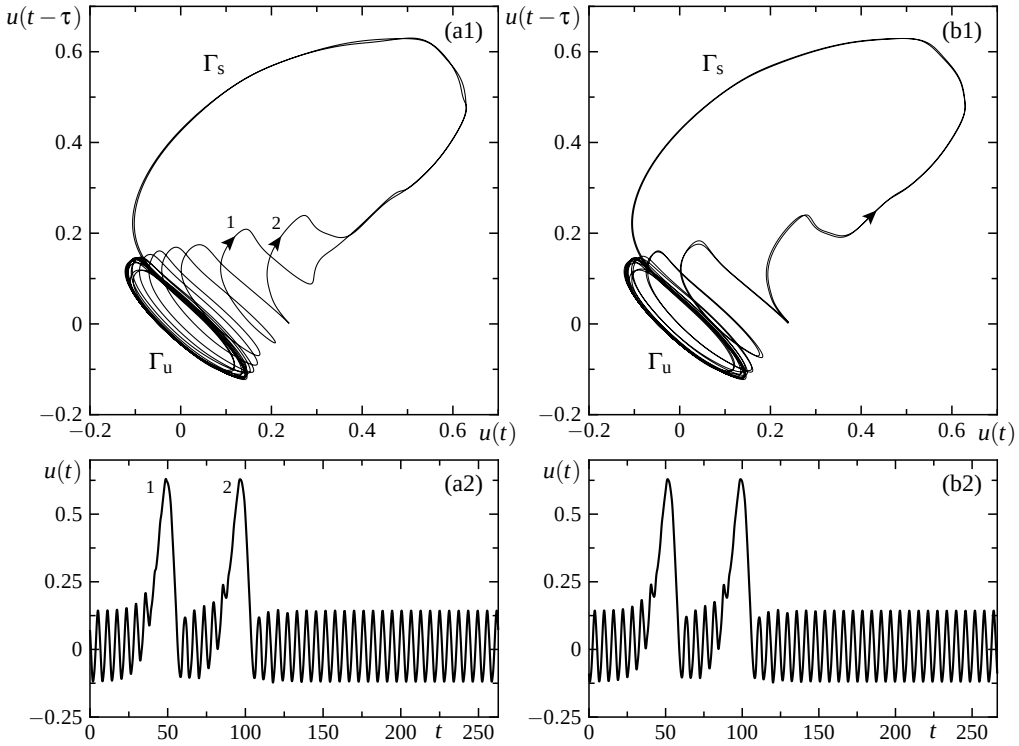

Figure 12. Phase-plane projections and time series of two multi-pulse periodic solutions, which are identical in the number of small and large oscillations they possess, but differ in the location where the trajectories leave the vicinity of Γ_u; compare points 1 and 2 in panel (a).

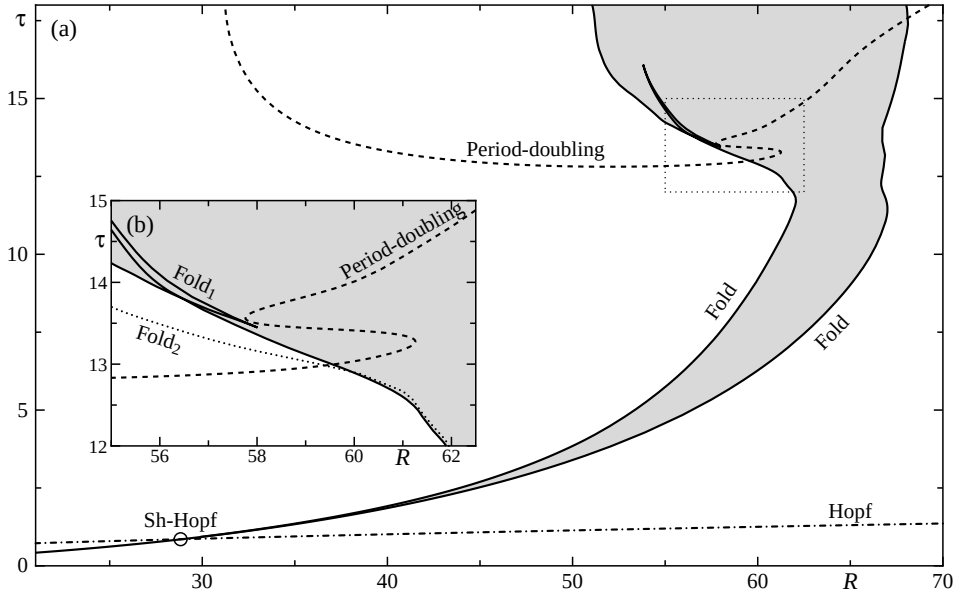

Figure 13. Two-parameter bifurcation diagram in the (R,τ)-plane. The solid curves are the folds of the snaking branch shown in figure 8(a), the dashed curve is a branch of period-doubling bifurcations of Γ_u, and the dash-dotted curve is a branch of Hopf bifurcations of Γ_u. Panel (b) shows an enlargement of the branches close to the curve of period-doubling bifurcations; at this point the two folds that have been continued (shown as solid and dotted curves) diverge, which indicates that the homoclinic tangency is no longer well approximated.

$(u(t),u(t-\tau))$-plane representations of two such multi-pulse solutions at the points marked (a) and (b) in figure 11. Both periodic solutions have the same number of small and large oscillations; the difference between them is the point at which the solution leaves the vicinity of the underlying periodic solution to make the global excursion. This difference in phase is clearly seen by comparing the points marked 1 and 2 in figure 12(a). In addition to the results presented here, we have found many more multi-pulse solutions, including three- and four-pulse solutions. All exhibit similar behaviour.

6. Continuation of homoclinic tangencies

In this section we extend the investigation of the homoclinic orbit of a periodic solution, described in section 5, to the two-parameter (R,τ)-plane. The domain of existence of the homoclinic orbit to Γ_u is defined by the associated homoclinic tangencies. As described in section 3.2, we continue a number of folds of the associated snaking branch of periodic solutions as an approximation to the homoclinic tangencies. In particular, we use the periodic solution in figure 8(d) and further solutions at the consecutive folds, shown in figure 8, as starting data.

Figure 13 shows the resulting bifurcation diagram in the (R,τ)-plane. The solid curves are the folds of the snaking branch, which bound the domain of existence of a robust homoclinic orbit (grey region). The other curves marked on figure 13 correspond to the bifurcations of the underlying periodic solution Γ_u; the dashed curve is a locus of period-doubling bifurcations and the dash-dotted curve is a locus of Hopf bifurcations. The one-parameter continuation shown in figure 8 corresponds to a horizontal slice through figure 13(a)

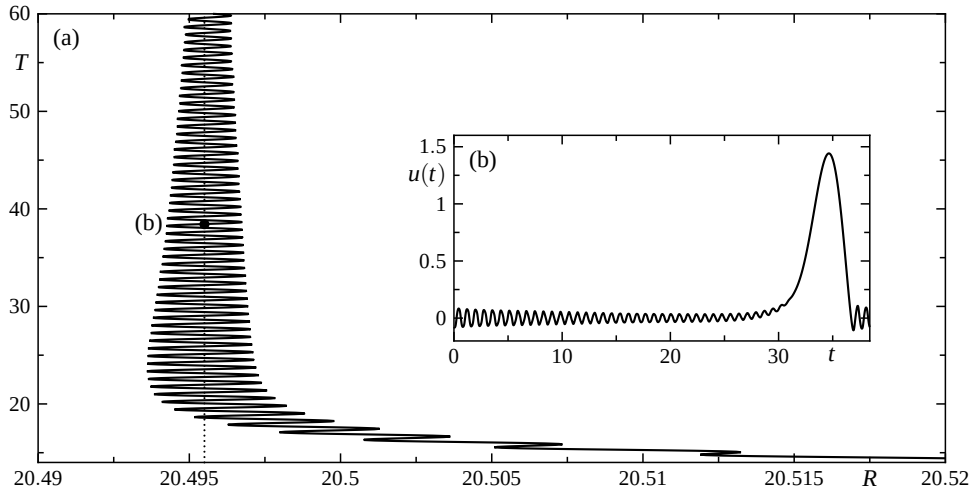

Figure 14. Panel (a) shows a branch of snaking periodic solutions for $\tau = 0.5$ in the (R,T)-plane, where T is the period of the solution. As the branch is followed in increasing T the range in R covered by the snaking branch decreases, indicating a homoclinic orbit of a steady-state. Panel (b) shows a periodic solution for $R = 20.495$.

at $\tau = 3.5$.

When τ is small, the folds marking the edge of the snaking region (the homoclinic tangencies) are close together in parameter space and so the domain of existence of the homoclinic orbit is small. At $\tau = \tau_{\text{Hopf}} := 0.854$ (labelled by a circle in figure 13) the fold curves cross the Hopf bifurcation curve of Γ_{u} and, consequently, there can no longer exist a homoclinic orbit of a periodic solution. Instead, the homoclinic orbit has been 'transfered' to the trivial steady-state u_0 at a codimension-two Shil'nikov-Hopf bifurcation. Thus, for $\tau < \tau_{\text{Hopf}}$ the fold curves approximate the codimension-one curve of homoclinic orbits of u_0. For larger values of τ the fold curves are well separated and the domain of existence of the homoclinic orbit is quite large. At large values of τ the fold curves cross the curve of period-doubling bifurcations of Γ_{u}. After this crossing the fold continuation no longer approximates the curve of homoclinic tangencies accurately, see figure 13(b). The dotted curve denotes the continuation of a second fold on the snaking branch shown in figure 8, and it clearly diverges from the first fold curve in the immediate vicinity of the period-doubling bifurcation. Thus, after the period-doubling curve has been crossed it is not clear how one can approximate the homoclinic tangency. We are also left with the question of what the homoclinic orbit is connected to: the period-one solution, the period-two solution or neither? We are not aware of any results specifically relating to this situation. However, in the context of robust heteroclinic orbits in maps it has been proved [43] that after the period-doubling the heteroclinic orbit is connected to the period-two solution.

The situation for robust homoclinic orbits in NDDEs remains an interesting open question. We now present a series of one-parameter continuations and some of the solutions on these branches that suggests that the situation is quite complicated. Figure 14(a) shows a branch of snaking periodic solutions for $\tau = 0.5 < \tau_{\text{Hopf}}$. It is similar in structure to the snaking branch in figure 8, with the exception that the snaking region shrinks as the branch is followed; this is indicative of a homoclinic orbit to a steady-state. The convergence of the folds to the parameter value at which the homoclinic orbit exists is predicted to be exponential. However, in figure 14(a) it appears to be very slow. Slow convergence is also seen in the

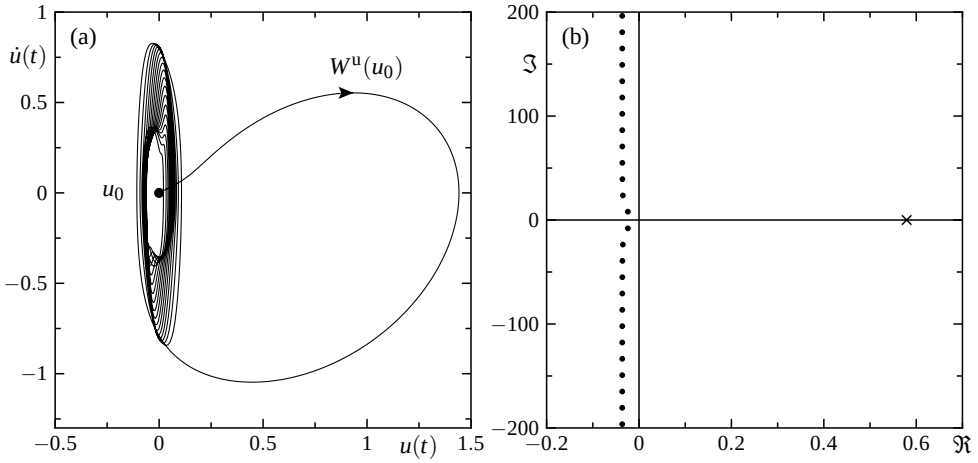

Figure 15. Panel (a) shows an approximation to the unstable manifold of u_0 for $R = 20.50$ and $\tau = 0.5$, which gives the homoclinic orbit. The trajectory leaves the vicinity of u_0 before returning and spiralling in towards u_0. Panel (b) shows the spectrum of u_0; it is of saddle-type with one unstable eigenvalue.

time series of the periodic solution in figure 14(b); the oscillations approach u_0 very slowly. Figure 15(a) shows the approximated one-dimensional unstable manifold of u_0 (and thus also the homoclinic orbit) computed by direct integration of (1). The convergence of the trajectory towards u_0 is so slow that numerical errors accumulate and cause the trajectory to be ejected away from u_0 before entering its immediate neighbourhood. The cause of this slow convergence is the fact that a part of the spectrum of u_0 is close to the imaginary axis, as is shown in figure 15(b). The essential spectrum appears to approach a vertical asymptote in the complex plane. Consequently, the stable manifold is only weakly stable. This type of slowness if convergence is not covered by ODE theory, but is a feature of the NDDE aspect of our problem.

Figure 16 shows a sequence of one-parameter continuations in R for fixed values of $\tau = 11$, 13, 14 and 16, respectively. The branch for $\tau = 11$ has a similar structure to the snaking branch shown in figure 8. The main difference is at the base of the branch (i.e. where the period is small) where the branch shown in figure 16(a) appears to be less regular. For $\tau = 13$, close to the period-doubling of Γ_{u}, the snaking branch takes on an alternating structure which also persists for $\tau = 14$. The snaking branch also appears to be even more complex and has many additional folds. For $\tau = 16$ the snaking branch is extremely complicated. In fact, it is not computationally tractable to continue them further.

Although we are unable to continue the branch shown in figure 16(d) any further, we are able to compute a solution with a high period for $\tau = 13$ and then continue it in τ until $\tau = 16$. After further continuation in R, the periodic solutions shown in figure 17 were found. Figure 17(a) shows a periodic solution for $R = 55.7$ where the limiting periodic solution appears to be the period-one solution. Further continuation studies (not presented here) reveals many more periodic solutions that repeatedly come close to the period-one solution. However, we have found no periodic solutions that approach the period-two solution. This is a strong indication that the homoclinic orbit remains connected to the period-one solution through the period-doubling bifurcation, in contrast to the situation described in [43]. Figure 17(b) shows a periodic solution, again for $R = 55.7$, where the underlying periodic solution is

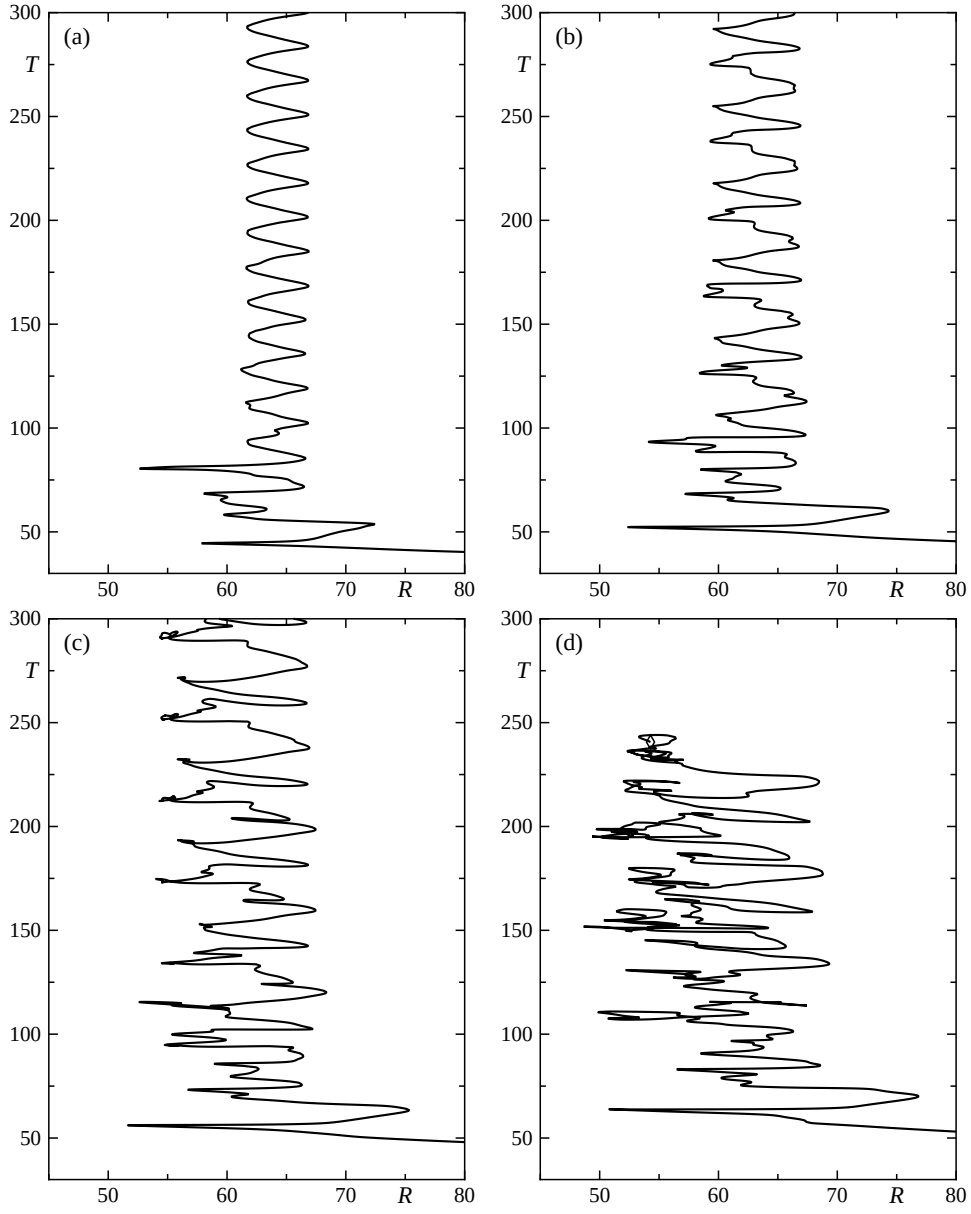

Figure 16. Branches of snaking solutions for $\tau = 11.0$, 13.0, 14.0 and 16.0 respectively. The continuation of the branch shown in panel (d) stops due to computational limits.

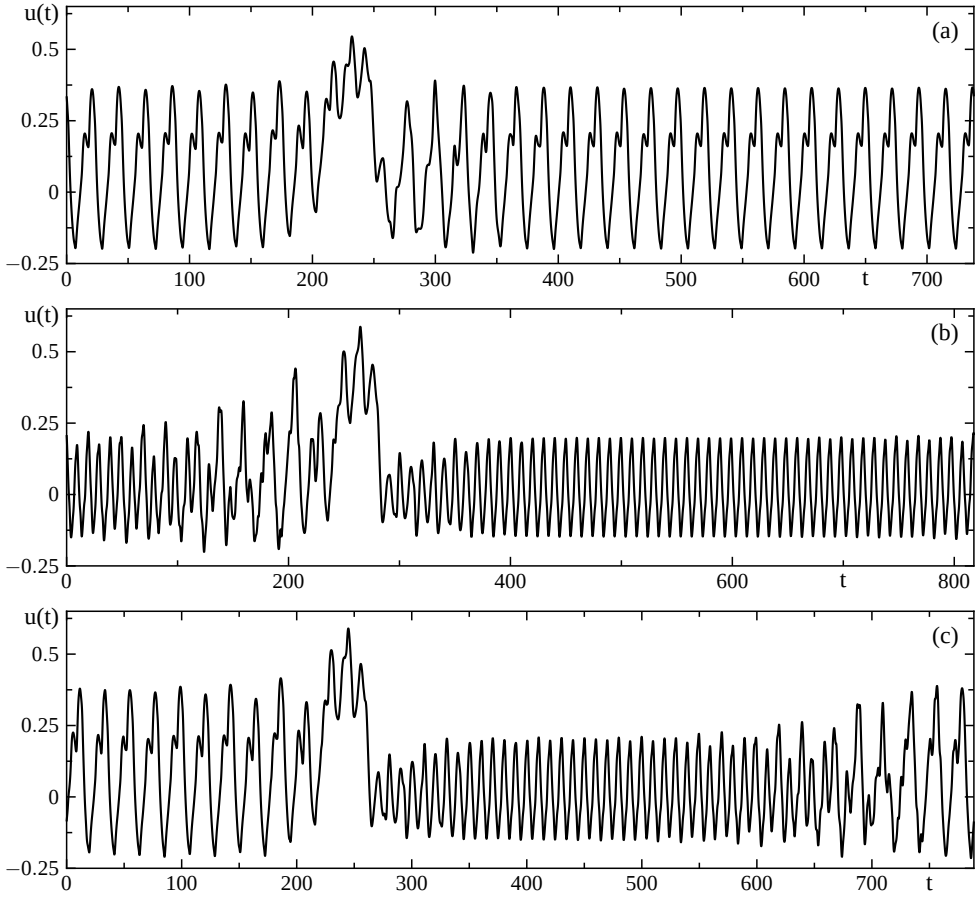

Figure 17. Periodic solutions for $R = 55.7$ in panels (a) and (b), and for $R = 52.8$ in panel (c); throughout $\tau = 16$. These solutions indicate the possibility of further homoclinic or heteroclinic connections.

different; it is neither the period-one nor period-two solution. Instead, it is a periodic solution on a branch that bifurcates from u_0 at a different Hopf bifurcation. This suggests that there exists a second homoclinic orbit in the vicinity of the first one. Furthermore, figure 17(c) for $R = 52.8$ shows a periodic solution that passes close to both of the limiting periodic orbits. Thus, there may also exist heteroclinic connections between the different periodic solutions. These periodic solutions strongly suggest that the complexity seen in the snaking branches of periodic solutions is not due to the period-doubling bifurcation of Γ_u. Instead, it appears that the complexity arises when other homoclinic orbits and/or heteroclinic connections are created nearby.

7. Conclusions

We have shown that the transmission line oscillator modelled by NDDE (1) possesses a wealth of delay-induced dynamics. Specifically, we have used recently developed numerical continuation routines for NDDEs to demonstrate that the dynamics is organised by homoclinic orbits. We found snaking branches of periodic solutions that accumulate on these homoclinic

orbits. For small time delay, there is a homoclinic orbit to a steady-state. However, beyond a codimension-two Shil'nikov-Hopf bifurcation the homoclinic orbit is connected to a periodic solution. As the time delay is increased there is a significant increase in the complexity of the snaking branches. This appears to coincide with a period-doubling bifurcation of the periodic solution underlying the homoclinic orbit. There is some evidence that the homoclinic orbit remains connected to the period-one solution. However, we also found evidence of further homoclinic/heteroclinic connections involving other periodic solutions. The exact structure of the bifurcations involved remains an interesting topic for future research.

Our case study of the TLO shows that much of the theory of homoclinic orbits in ODEs transfers directly to NDDEs. However, there are peculiarities that are due to the NDDE nature of the problem. In particular, we find that some convergence rates of the fold points in homoclinic snaking are substantially slower than those arising in ODE systems. We attribute this effect to the essential spectrum, which forms a vertical asymptote in the complex plane close to the imaginary axis.

More generally, bifurcation analysis tools for NDDEs are now able to reveal a great deal of useful information about the system in question. Our case study of a TLO demonstrates that these tools allow one to investigate even quite complicated dynamics and bifurcations of NDDE models arising in applications. In the future we plan to study NDDE models of dynamic substructuring tests [44]. In this hybrid test set-up, where a physical experiment is bi-directionally coupled to a computer simulation, the delay is due to coupling delays and the finite response times of actuators. Neutrality of the model arises when velocity information is used as part of the feedback loop.

References

[1] A.N. Sharkovsky. Chaos from a time-delayed Chua's circuit. *Circuits and Systems I: Fundamental Theory and Applications*, 40(10):781–783, 1993.

[2] J. Kawata, Y. Nishio, and A. Ushida. Analysis of Chua's circuit with transmission line. *Circuits and Systems I: Fundamental Theory and Applications*, 44(6):556–558, 1997.

[3] R.K. Brayton. Nonlinear oscillations in a distributed network. *Quarterly of Applied Mathematics*, 24(4):289–301, 1967.

[4] R.K. Brayton. Bifurcation of periodic solutions in a nonlinear difference-differential equation of neutral type. *Quarterly of Applied Mathematics*, 24(3):215–224, 1966.

[5] W.L. Miranker. Periodic solutions of the wave equation with a nonlinear interface condition. *IBM Journal of Research and Development*, 5(1):2–24, 1961.

[6] J.N. Blakely and N.J. Corron. Experimental observation of delay-induced radio frequency chaos in a transmission line oscillator. *Chaos*, 14(4):1035–1041, 2004.

[7] J.N. Blakely, J.D. Holder, N.J. Corron, and S.D. Pethel. Simply folded band chaos in a VHF microstrip oscillator. *Physics Letters A*, 346(1–3):111–114, 2005.

[8] I. Fischer, Y. Liu, and P. Davis. Synchronization of chaotic semiconductor laser dynamics on subnanosecond time scales and its potential for chaos communication. *Physical Review A*, 62(1):011801, 2000.

[9] S. Hayes, C. Grebogi, and E. Ott. Communicating with chaos. *Physical Review Letters*, 70(20):3031–, 1993.

[10] K. Myneni, T.A. Barr, B.R. Reed, S.D. Pethel, and N.J. Corron. High-precision ranging using a chaotic laser pulse train. *Applied Physics Letters*, 78(11):1496–1498, 2001.

[11] O. Diekmann, S. van Gils, S.M.V. Lunel, and H.-O. Walther. *Delay equations: functional, complex, and nonlinear analysis*, volume 110 of *Applied Mathematical Sciences*. Springer, New York, 1995.

[12] K. Engelborghs, D. Roose, and T. Luzyanina. Bifurcation analysis of periodic solutions of neutral functional differential equations: a case study. *International Journal of Bifurcation and Chaos*, 8(10):1889–1905, 1998.

[13] K. Engelborghs and D. Roose. Smoothness loss of periodic solutions of a neutral functional-differential equation: on a bifurcation of the essential spectrum. *Dynamics and Stability of Systems*, 14(3):255–273, 1999.

[14] O. Lopes. Forced oscillations in nonlinear neutral differential equations. *SIAM Journal on Applied Mathematics*, 29(1):196–207, 1975.

[15] S. Chowdhury, J.S. Barkatullah, D. Zhou, E.-W. Bai, and K.E. Lonngren. A transmission line simulator for high-speed interconnects. *IEEE Transactions on Circuits and Systems II*, 39(4):201–211, 1992.

[16] E.J. Doedel, A.R. Champneys, T.F. Fairgrieve, Y.A. Kuznetsov, B. Sandstede, and X. Wang. *AUTO 97: Continuation and bifurcation software for ordinary differential equations*, 1998.

[17] K. Engelborghs, T. Luzyanina, and G. Samaey. DDE-BIFTOOL v. 2.00: a Matlab package for bifurcation analysis of delay differential equations. Technical Report TW330, Department of Computer Science, K.U. Leuven, Leuven, Belgium, 2001.

[18] R. Szalai. *PDDE-CONT: A continuation and bifurcation software for delay-differential equations*, 2005. http://www.mm.bme.hu/˜szalai/pdde/.

[19] D.A.W. Barton, B. Krauskopf, and R.E. Wilson. Collocation schemes for periodic solutions of neutral delay differential equations. Journal of Difference Equations and Applications, 2006, in press. (http://www.enm.bris.ac.uk/anm/preprints/2005r31.html).

[20] D.A.W. Barton. Files for continuation of neutral delay differential equations in DDE-BIFTOOL. http://www.cityinthesky.co.uk/ndde.html, 2005.

[21] L. Corti, L. de Menna, G. Miano, and L. Verolino. Chaotic dynamics in an infinite-dimensional electromagnetic system. *IEEE Transactions on Circuits and Systems I*, 41(11):730–736, 1994.

[22] J.K. Hale and S.M. Verduyn Lunel. *Introduction to functional differential equations*. Number 99 in Applied Mathematical Sciences. Springer, 1993.

[23] G.W. Hunt, M.A. Peletier, A.R. Champneys, P.D. Woodsand, M. Ahmer Wadee, C.J. Budd, and G.J. Lord. Cellular buckling in long structures. *Nonlinear Dynamics*, 21(1):3–29, 2000.

[24] G.W. Hunt. Buckling in space and time. *Nonlinear Dynamics*, 43(1–2):29–46, 2006.

[25] S. Coombes, G. J. Lord, and M. R. Owen. Waves and bumps in neuronal networks with axo-dendritic synaptic interactions. *Physica D*, 178(3-4):219–241, 2003.

[26] M. Chen. Solitary-wave and multi-pulsed travelling-wave solutions of Boussinesq systems. *Applicable Analysis*, 75(1–2):213–240, 2000.

[27] D.V. Skryabin and A.R. Champneys. Walking cavity solitons. *Physical Review E*, 63(6):066610, 2001.

[28] Y.A. Kuznetsov. *Elements of applied bifurcation theory*. Number 112 in Applied Mathematical Sciences. Springer, 2nd edition, 1998.

[29] J. Guckenheimer and P. Holmes. *Nonlinear oscillations, dynamical systems, and bifurcations of vector fields*. Number 42 in Applied Mathematical Sciences. Springer-Verlag, New York, 1983.

[30] S. Wiggins. *Global bifurcations and chaos*, volume 73 of *Applied Mathematical Sciences*. Springer-Verlag, New York, 1988.

[31] P. Hirschberg and E. Knobloch. Šil'nikov-Hopf bifurcation. *Physica D*, 62(1–4):202–216, 1993.

[32] P. Gaspard and X.J. Wang. Homoclinic orbits and mixed-mode oscillations in far-from-equilibrium systems. *Journal of Statistical Physics*, 48(1–2):151–199, 1987.

[33] S. Wieczorek and B. Krauskopf. Bifurcations of *n*-homoclinic orbits in optically injected lasers. *Nonlinearity*, 18(3):1095–1120, 2005.

[34] R. Seydel. *Practical bifurcation and stability analysis*. Springer, New York, 1994.

[35] E.J. Doedel, H.B. Keller, and J.P. Kernevez. Numerical analysis and control of bifurcation problems, part I. *International Journal of Bifurcation and Chaos*, 1(3):493–520, 1991.

[36] E.J. Doedel, H.B. Keller, and J.P. Kernevez. Numerical analysis and control of bifurcation problems, part II. *International Journal of Bifurcation and Chaos*, 1(4):745–772, 1991.

[37] Y.A. Kuznetsov and V.V. Levitin. CONTENT: A multi-platform environment for continuation and bifurcation analysis of dynamical systems. Technical report, Centrum voor Wiskunde en Informatica, Amsterdam, The Netherlands, 1997.

[38] M.A. Heroux, R.A. Bartlett, V.E. Howle, R.J. Hoekstra, J.J. Hu, T.G. Kolda, R.B. Lehoucq, K.R. Long, R.P. Pawlowski, E.T. Phipps, A.G. Salinger, H.K. Thornquist, R.S. Tuminaro, J.M. Willenbring, A. Williams, and K.S. Stanley. An overview of the Trilinos project. *ACM Transactions on Mathematical Software*, 31(3):397–423, 2005.

[39] G. Samaey, K. Engelborghs, and D. Roose. Numerical computation of connecting orbits in delay differential equations. *Numerical Algorithms*, 30(3–4):335–352, 2002.

[40] N. Guglielmi and E. Hairer. Implementing Radau IIA methods for stiff delay differential equations. *Computing*, 67(1):1–12, 2001.

[41] N. Guglielmi and E. Hairer. Users' guide for the code RADAR5 - version 2.1. Technical report, Università dell'Aquila, Italy, 2005.

[42] N. Guglielmi and E. Hairer. Automatic computation of breaking points in implicit delay differential equations. Preprint. http:// www.unige.ch/˜hairer/preprints.html, 2005.

[43] T. Hüls. Bifurcation of connecting orbits with one nonhyperbolic fixed point for maps. *SIAM Journal on Applied Dynamical Systems*, 4(4):985–1007, 2005.

[44] Y.N. Kyrychko, K.B. Blyuss, A. Gonzalez-Buelga, S.J. Hogan, and D.J. Wagg. Real-time dynamic substructuring in a coupled oscillator-pendulum system. *Proceedings of the Royal Society A*, 462:1271–

1294, 2006.